Supplementary Information

Syntheses, structures and luminescence properties of novel metal-organic frameworks based on zinc(II), cadmium(II) or lead(II) and a 2,2'-dimethoxy-functionalised biphenyl linker†

Witri Wahyu Lestari,[a] Peter Lönnecke,[a] Menyhárt B. Sárosi,[b] Huayna Cerqueira Streit,[c] Matthias Adlung,[c] Claudia Wickleder,[c] Marcel Handke,[a] Wolf-Dietrich Einicke,[d] Roger Gläser,[d] and Evamarie Hey-Hawkins*[,a]

[a] *Institut für Anorganische Chemie, Fakultät für Chemie und Mineralogie, Universität Leipzig, Johannisallee 29, D-04103 Leipzig, Germany. Email: hey@rz.uni-leipzig.de*

[b] *Departamentul de Chimie, Facultatea de Chimie şi Inginerie Chimică, Universitatea Babeş-Bolyai, Str. M. Kogălniceanu Nr. 1, RO-400084, Cluj-Napoca, Romania*

[c] *Anorganische Chemie II, Fakultät IV, Department Chemie-Biologie, Universität Siegen, Adolf-Reichwein-Straße, D-57068 Siegen, Germany.*

[d] *Institut für Technische Chemie, Fakultät für Chemie und Mineralogie, Universität Leipzig, Linnéstr. 3, D-04103 Leipzig, Germany.*

TABLE OF CONTENTS

1. Ligand synthesis (LH_2) 2
2. Theoretical calculations 4
3. TGA Measurements of Compounds **1**, **2**, and **3** 7
4. X-ray powder diffraction studies 9
5. Nitrogen Adsorption Isotherms at 77 K 12

1. Ligand synthesis (LH_2)

The synthesis of 4,4´-$(CO_2H)_2$-2,2´-$(OMe)_2$-1,1´-$(C_6H_3)_2$ (**LH_2**) was reported before.[1] A modified synthesis by Wöckel (2007)[2] is reported below. The iron-catalysed oxidative homo-coupling reaction via aryl Grignard reagent was performed under nitrogen using Schlenk technique and dry solvents. ^{1}H and ^{13}C NMR spectra were recorded on an AVANCE DRX 400 spectrometer (Bruker). The chemical shifts for ^{1}H and ^{13}C NMR spectra are reported in parts per million (ppm) at 400.13 MHz, and 100.63 MHz, respectively, with tetramethylsilane as standard and measured at 298 K. Mass spectra were recorded with a VG ZAB HSQ Analytical Manchester.

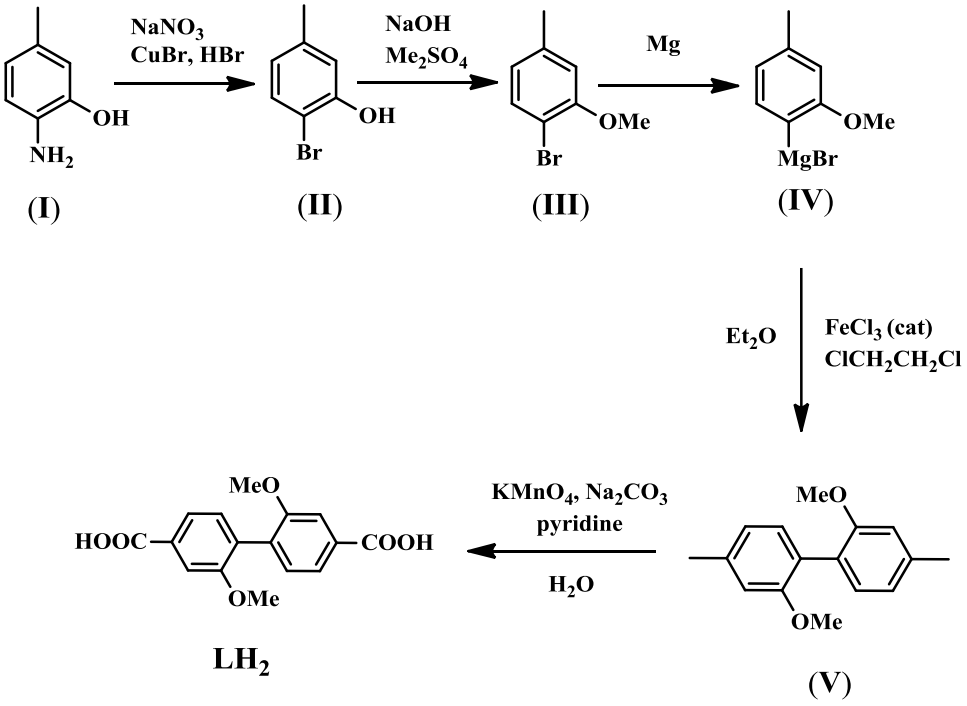

Scheme 1. Synthesis of 4,4´-$(CO_2)_2$-2,2´-$(OMe)_2$-1,1´-$(C_6H_3)_2$.

As starting material, commercially available 2-amine-5-methyl-phenol (**I**) was used without further purification. Compound **II** was prepared following reported procedures.[3,4] Protection of the OH group (compound **III**) as –OMe group was conducted following the literature.[5] Iron-catalyzed oxidative homocoupling reaction via aryl Grignard reagent **IV** to obtain compound **V** was done according to the literature.[6,7] Compound **V** was isolated as colourless crystals from diethyl ether and characterised also by single crystal X-ray diffraction studies. Compound **5** crystallises in the orthorhombic space group *F*dd2 (Figure 1). CCDC 911251 (**V**) contains the supplementary crystallographic data for this paper. These data can be

obtained free of charge from The Cambridge Crystallographic Data Centre via www.ccdc.cam.ac.uk/data_request/cif. The Crystallographic data for compound (V) is listed in Table1.

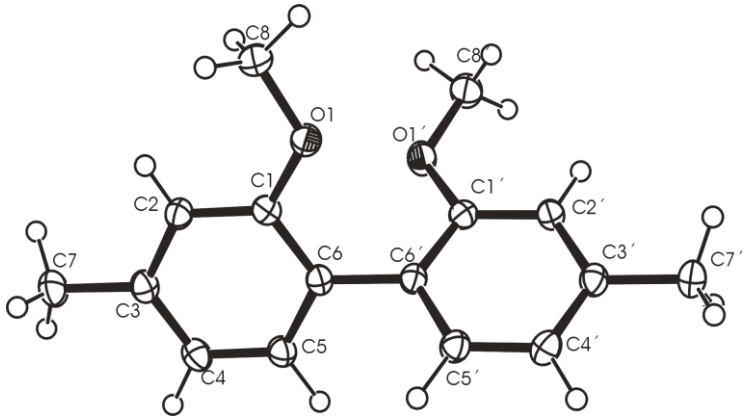

Figure 1. ORTEP representation of compound **V**.

Table 1. Crystallographic data for compound **V**

Formula	$C_{16}\ H_{18}\ O_2$
FW	242.30
Temp./K	130(2) K
Crystal system	Orthorhombic
Space group	*F*dd2
a/Å	15.1458(6)
b/Å	20.2514(9)
c/Å	86.838(4)
α/°	90
β/°	90
γ/°	90
V(Å^3)	2663.5(2)
Z	8
D_c/Mg m^{-3}	1.208
F(000)	1040
Reflns collected	3551
Independent reflns	1073
R_{int}	0.0196
GOF on F^2	1.039
R1, wR_2[I>2σ(I)]	0.0376, 0.1039
R1, wR_2 (all data)	0.0429, 0.1061

Compound **V** was dissolved in pyridine. The oxidation method that was used is a combination of two published procedures (by Hòly et al.[8] and Dickie et al.[9]) to obtain the product (**LH_2**) which was isolated as a white solid. Details of the synthesis are given below.

1.1. Synthesis of Biphenyl-2,2´-dimethoxy-4,4´-dicarboxylic acid (LH_2)

Compound **V** (2.72 g, 11.29 mmol) was dissolved in pyridine (27.8 mL) and the solution refluxed for 10–15 minutes. 11.94 g (75.34 mmol) $KMnO_4$ and 8.79 g (82.90 mmol) Na_2CO_3 were dissolved in H_2O (111 mL) and the reaction mixture was heated at 70 ºC. This solution was added dropwise to the pyridine solution at room temperature. The colour changed from bright yellow to dark brown-violet. The reaction mixture was refluxed for 5 h. The solution was cooled to room temperature. Excess $KMnO_4$ was destroyed by addition of $NaHSO_3$ solution (added until a colourless solution had formed (ca 100 mL)). The solid brown material was isolated by filtration. The clear solution was cooled at 0 °C. Concentrated hydrochloric acid was added dropwise until pH 1 (ca. 52 mL) to precipitate the desired compound. The white solid was filtered off, and washed with cold water, until a neutral pH was reached. The resulting white solid was dried in air. Yield: 2.21 g (7.25 mmol; 64 %)

Characterization:

^{1}H NMR (d_6-DMSO, ppm); δ = 3.77 (s, 6H, OCH_3), 7.28 (d, $^3J_{HH}$ = 7.7 Hz, 2H, H-6/H-6´), 7.58 (m, 4H, H-3/H-3´ and H-5/H-5´), 13.00 (br, 2H, COOH)

IR (KBr, cm^{-1}): $\tilde{\nu}$ = 3432 (br); 2964 (s, ν(O–H)); 2647 (w); 1687 (s, ν(C=O)); 1604, 1575 (m-s, C=C); 1456 (s); 1417 (s); 1288, (s, ^{C}ν(C–O)); 1260 (w, ^{M}ν(C–O)); 1183 (w); 1117 (m); 1038 (st), 1005 (m); 910 (w); 877 (m); 811 (w); 759 (s); 658 (w); 528 (w).

Note: the C–O vibration of the methoxy group, it is denoted ^{M} and the carboxylic C–O is denoted ^{C}. MS (ESI): *m/z* = 303.10; calcd. for $[C_{16}H_{14}O_6H]^+$: 303.08

2. Theoretical calculations

All calculations were carried out in the gas phase with the M06 density functional[10] of the Gaussian 09 program package[11] and using the 6-31+G(d,p) basis set for all atoms.

The relaxed potential energy surface (PES) scan along the θ(C1–C2–C3–C4) dihedral angle of **LH_2** revealed that the global minimum **S** isomer and the local minimum **R** isomer are connected through a very flat PES. The maximum connecting the **S** and **R** isomers lies only

~4 kJ mol^{-1} above the global minimum (Figure 2). Geometry optimisations starting from coordinates taken from the PES scan showed that the **R** isomer lies only a few kJ mol^{-1} above the **S** isomer (Table2). The transition state connecting the two structures has been located with the synchronous transit-guided quasi-Newton (STQN) method[12] and gave an activation energy of only 4.1 kJ mol^{-1} (Table 2). These results indicate that the rotation along the dihedral angle θ(C1–C2–C3–C4) of **LH_2** between **S** and **R** enantiomers is practically unhindered.

The experiments showed that θ = ~86° in $[\{(Zn_4O)(L)_3(H_2O)\}\cdot 4.5DMF]_n$ (**1**) and the emission spectrum of **1** is identical with the spectrum of **LH_2** but differs from the spectra of $[\{(Cd_3L_4)_2(CdL_2)\}\cdot 8DMF\cdot 8Me_2NH_2^+\cdot 2Cl^-]_n$ (**2**) and $[\{(Pb_6O_2)L_4\}\cdot 2EtOH]_n$ (**3**) (see article for details). Prompted by these results, the intermediate geometry **IM** with θ = 90.4° was taken from the PES scan and its properties have been also calculated. The dihedral angle of **IM** is close to the value found in **1**, while θ = ~60° in **S** and θ = ~120° in **R** (Table 2). Frequency calculations revealed **IM** as a local minimum without any imaginary frequencies lying at somewhat higher relative energy values than **S** and **R** isomers. However, the thermodynamic corrections to the total energy revealed **IM** as the global minimum (Table). Thus, no clearly preferred conformation can be identified for **LH_2** and it is highly probable that under different conditions **LH_2** and its metal complexes could adopt stable conformations with different dihedral angles θ, as indicated by the experimental results.

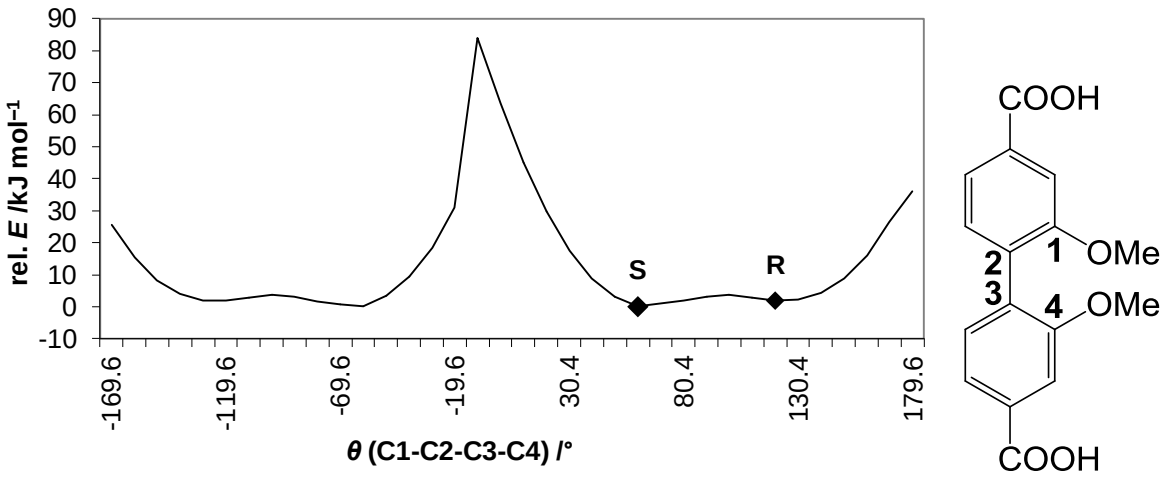

Figure 2. M06/6-31+G(d,p) relaxed potential energy surface (PES) scan of the full 360° rotation along the dihedral angle θ(C1–C2–C3–C4) with a step size of 10°. The critical points **S** and **R** are highlighted.

Table 2. Total energies (E) with corrections for zero point vibrations (E_{ZPE}) and the corresponding relative energies, HOMO-LUMO gaps (E_{gap}), θ(C1–C2–C3–C4) dihedral angle values, number of imaginary frequencies (Imags), point groups (Symm.) and relative Gibbs free energies (rel. G) of the optimised geometries.

	E [a.u.]	rel. E [kJ mol^{-1}]	E_{ZPE} [a.u.]	rel. E_{ZPE} [kJ mol^{-1}]	E_{gap} [eV]	θ [°]	Imags [cm^{-1}]	Symm.	rel. G [kJ mol^{-1}]
S	–1068.912304	0.0	–1068.635687	0.0	4.8	63.3	–	C_2	1.5
R	–1068.911468	2.2	–1068.634349	3.5	4.7	123.7	–	C_2	3.9
IM	–1068.911010	3.4	–1068.634754	2.4	5.3	90.4	–	C_1	0.0
TS	–1068.910742	4.1	–1068.634786	2.4	5.2	96.7	29i	C_2	5.6

The UV-VIS spectra of **S**, **R** and **IM** have also been calculated with the time-dependent DFT method. The first singlet excited states of both **S** and **R** correspond to the HOMO → LUMO transition and exhibit bands at 314 and 319 nm, respectively. However, the first excited state of **IM** has contributions from both the HOMO → LUMO and the HOMO–1 → LUMO+1 transitions and the corresponding wavelength is significantly shorter (289 nm) than the wavelengths calculated for **S** and **R**. The HOMO–1 and HOMO and the LUMO and LUMO+1 of **IM** form degenerate orbital pairs (Figure 4). Thus, the calculations are in agreement with the experimental observations and predict that conformations of **LH_2** with dihedral angles θ(C1–C2–C3–C4) around 60° give signals at lower wavenumbers than conformations with θ values around 90°. According to the above discussed results, it is highly probable that **LH_2** crystallises with a dihedral angle θ around 90°, giving an emission spectrum identical to the spectrum of 1, as shown by our luminescence measurements.

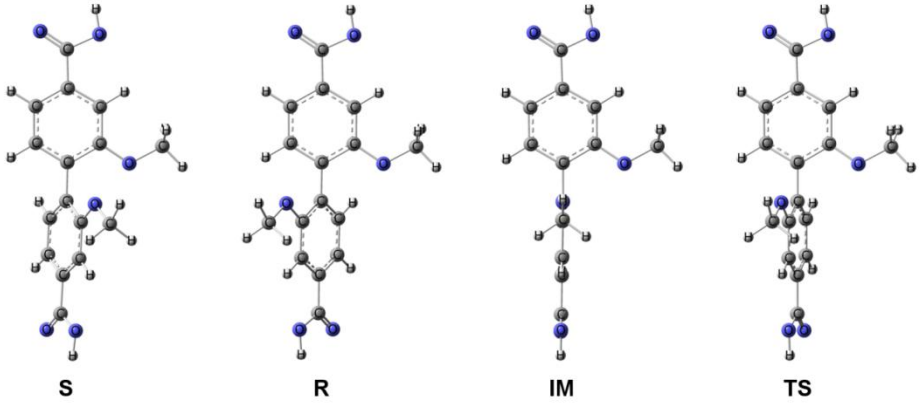

Figure 3. M06/6-31+G(d,p) optimised geometries.

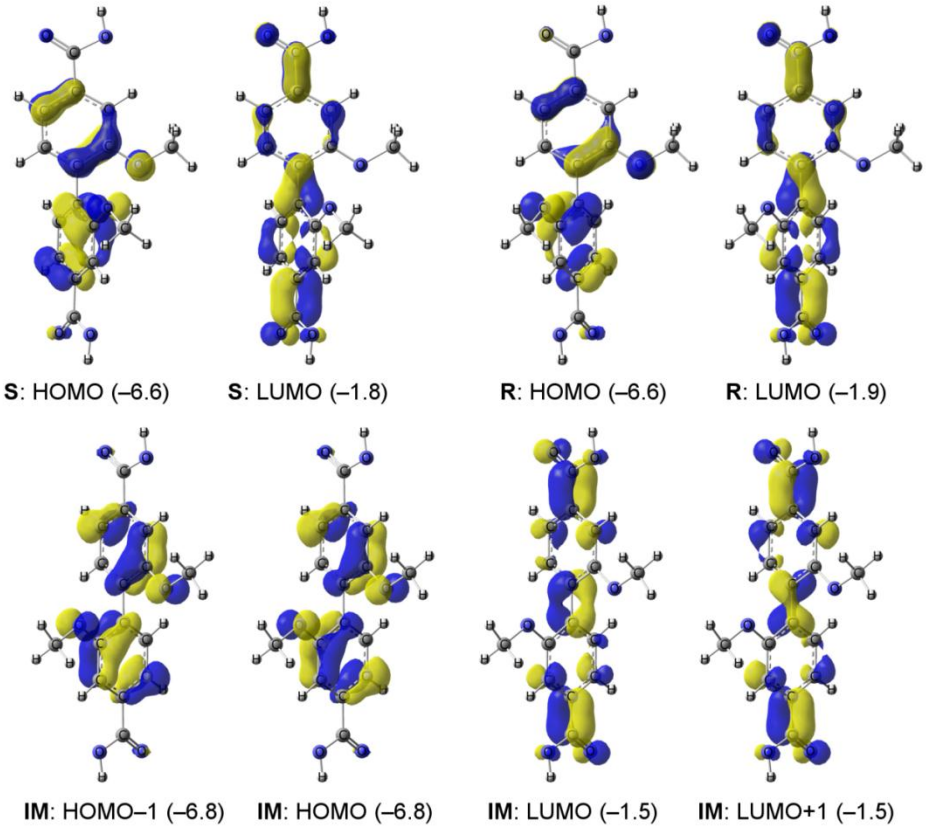

Figure 4: Molecular orbitals involved in the singlet transitions of **S**, **R** and **IM** (orbital energies in parentheses, in eV).

3. TGA Measurements of Compounds 1, 2, and 3

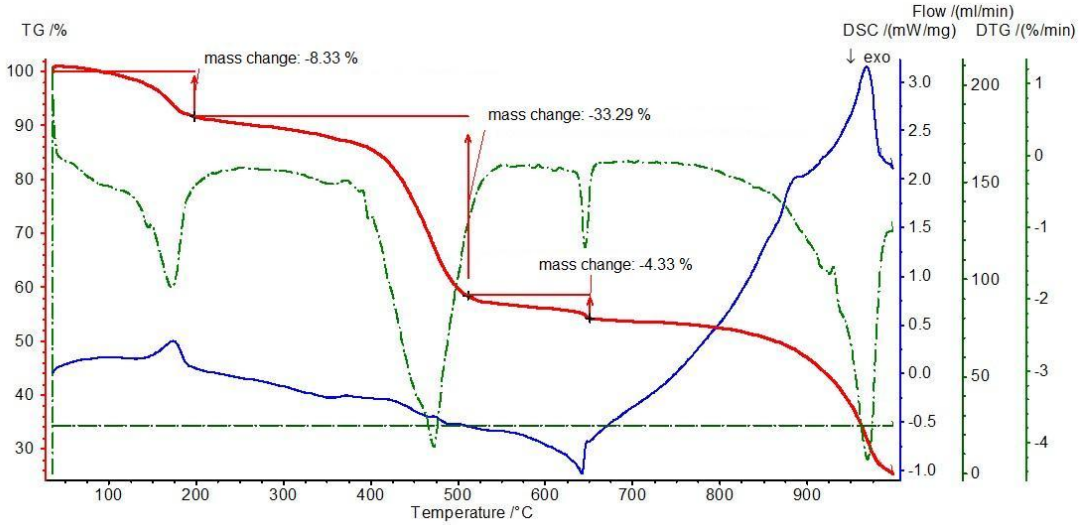

Figure 5. Thermogravimetric analysis (TGA) curve for Zn-based MOF **1**. The sample was heated to 900 ºC at a heating rate of 10 ºC/min.

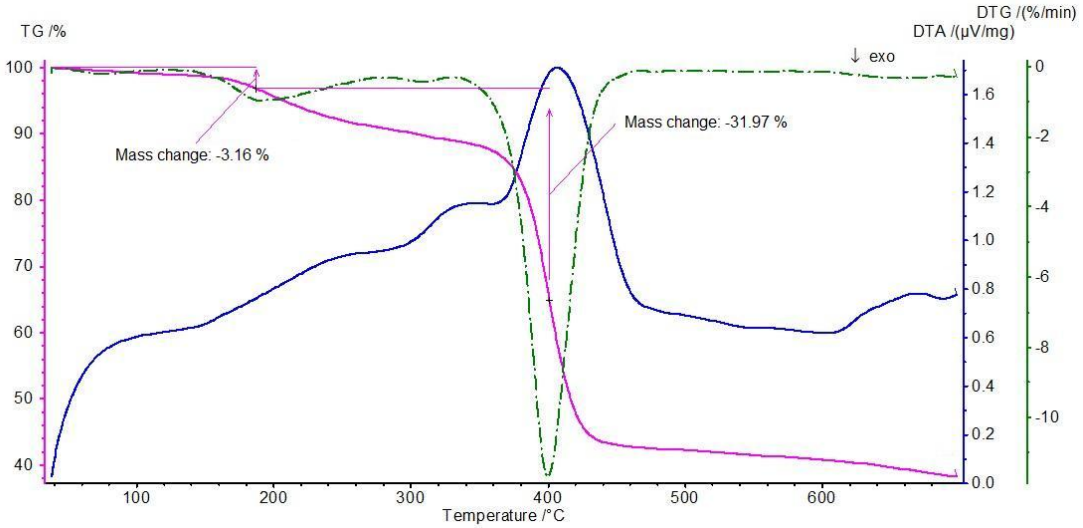

Figure 6. Thermogravimetric analysis (TGA) curve for Cd-based MOF **2**.
The sample was heated to 600 ºC at a heating rate of 10 ºC/min.

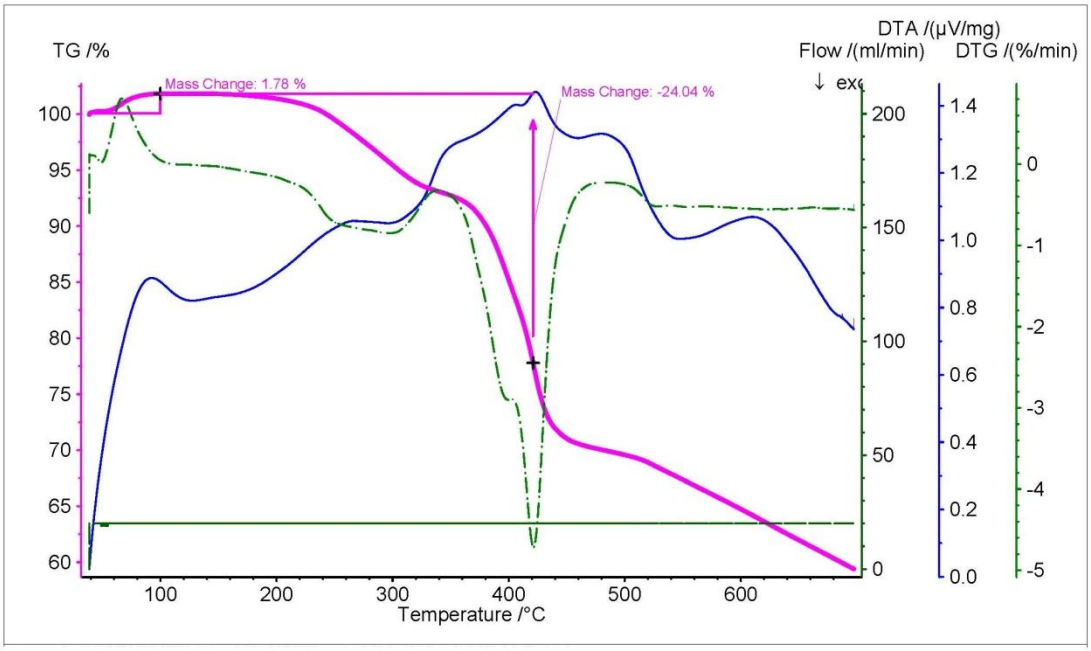

Figure 7. Thermogravimetric analysis (TGA) curve for Pb-based MOF **3**.
The sample was heated to 600 ºC at a heating rate of 10 ºC/min.

4. X-ray Powder Diffraction Studies

4.1. Zn-based MOF 1

Solvothermal synthesis and reflux were used for the of Zn-based MOF **1**. The characterisation was carried out with PXRD at room temperature. The PXRD pattern of the product obtained under solvothermal conditions is shown in Figure 8. The observed peaks are in agreement with the powder pattern of single crystals of **1**. An attempt to upscale the synthesis using the reflux method with the same stoichiometry but without addition of NEt_3 was carried out and the product was also studied by PXRD (Figure 9). The observed signals in the PXRD diagram are still the same as those of the single crystals but they are broader. In comparison to the PXRD diagram of the product obtained under solvothermal conditions, the latter exhibits superior crystallinity. The peaks are sometimes slightly shifted because of the different temperature employed in the measurement of the single crystals and the powder.

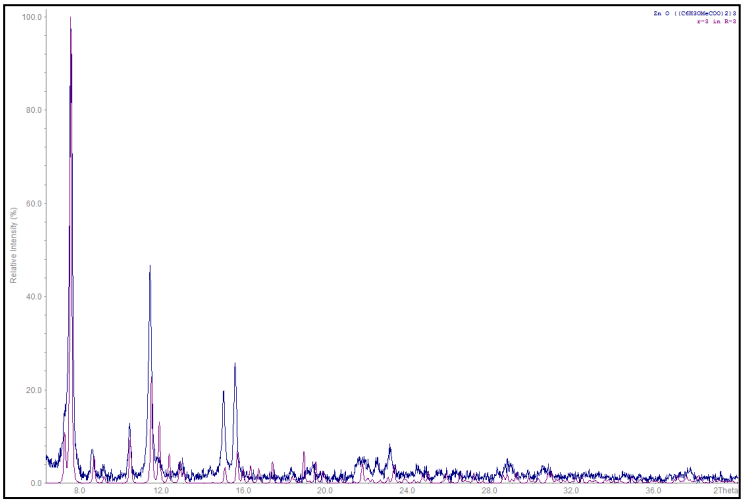

Figure 8. PXRD of the bulk product **1** obtained under solvothermal conditions (blue) indicating superior crystallinity. Red: simulated pattern from X-ray data.

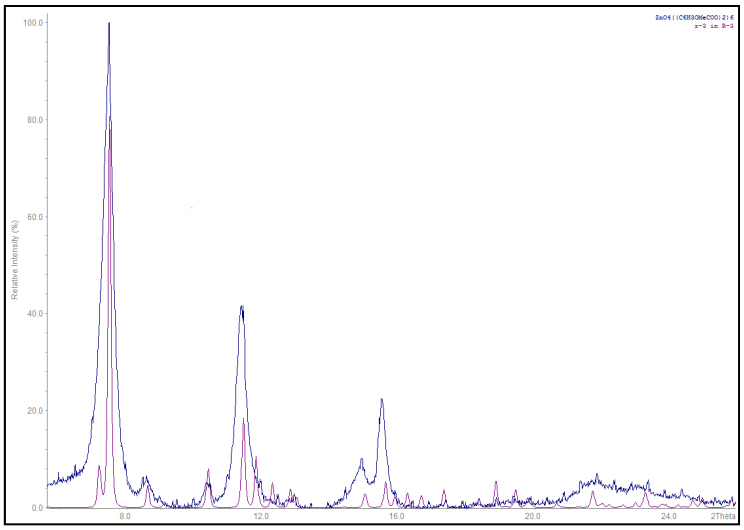

Figure 9. PXRD of the bulk product **1** obtained using the reflux method (blue) indicating lower crystallinity. Red: simulated pattern from X-ray data.

4.2. Thermal Stability Test of 1

A thermal stability test of **1** was carried out with PXRD. No changes were observed until 380 ºC. At 420 ºC, decomposition was observed. The new signals could be assigned to ZnO (according to the ICSD database).[13] Figure 10 (top view) and Figure 11 (3D views) illustrate these studies.

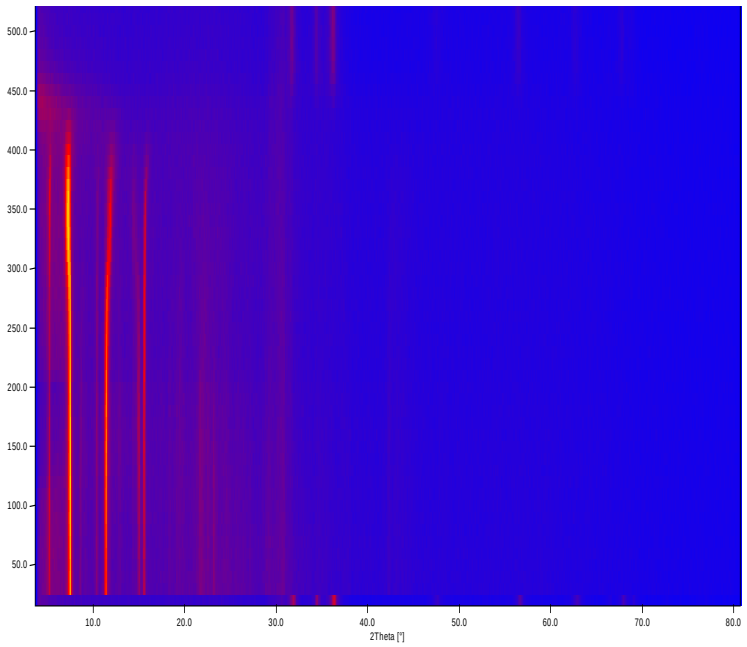

Figure 10. Top view of the PXRD diagram; heating from room temperature to 540 °C.

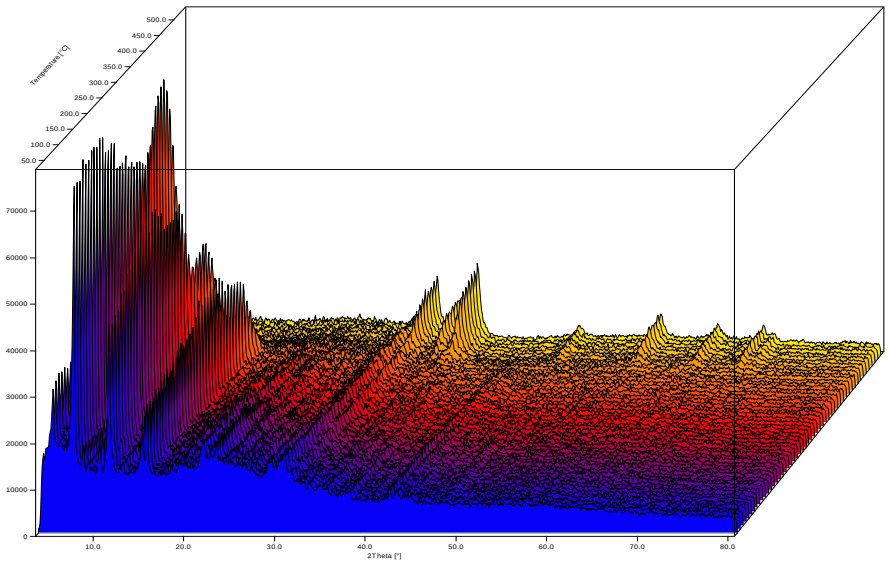

Figure 11. 3D view of the PXRD diagram; heating from room temperature to 540 °C.

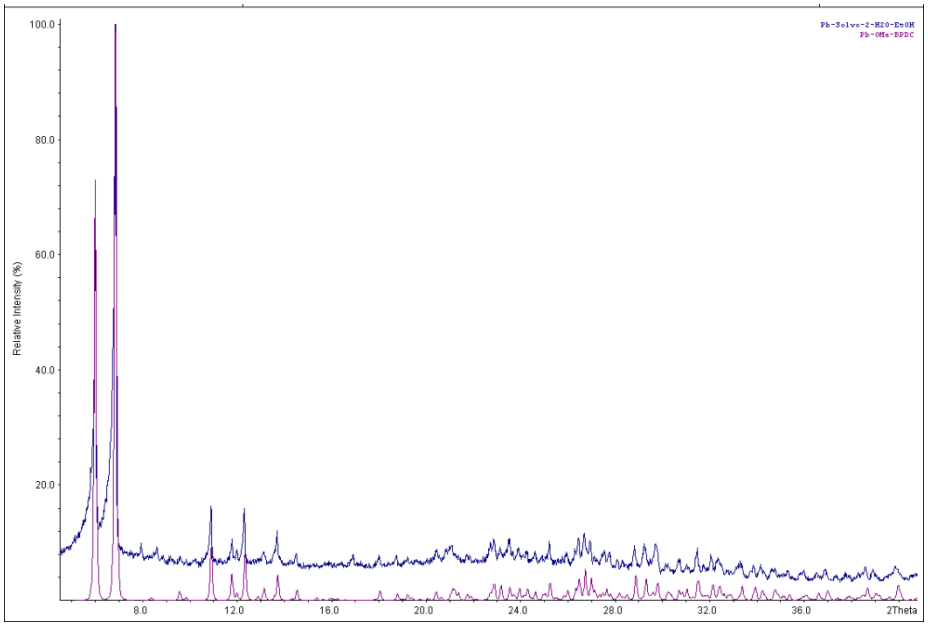

Figure 12. PXRD of the bulk product **3** obtained under solvothermal conditions (blue). Red: simulated pattern from X-ray data.

5. Nitrogen Adsorption Isotherms at 77 K

Figure 13. Nitrogen adsorption isotherms of **1** obtained from solvothermal synthesis (red) and at room temperature (black).

shows the nitrogen adsorption isotherm of **1** obtained from solvothermal synthesis.

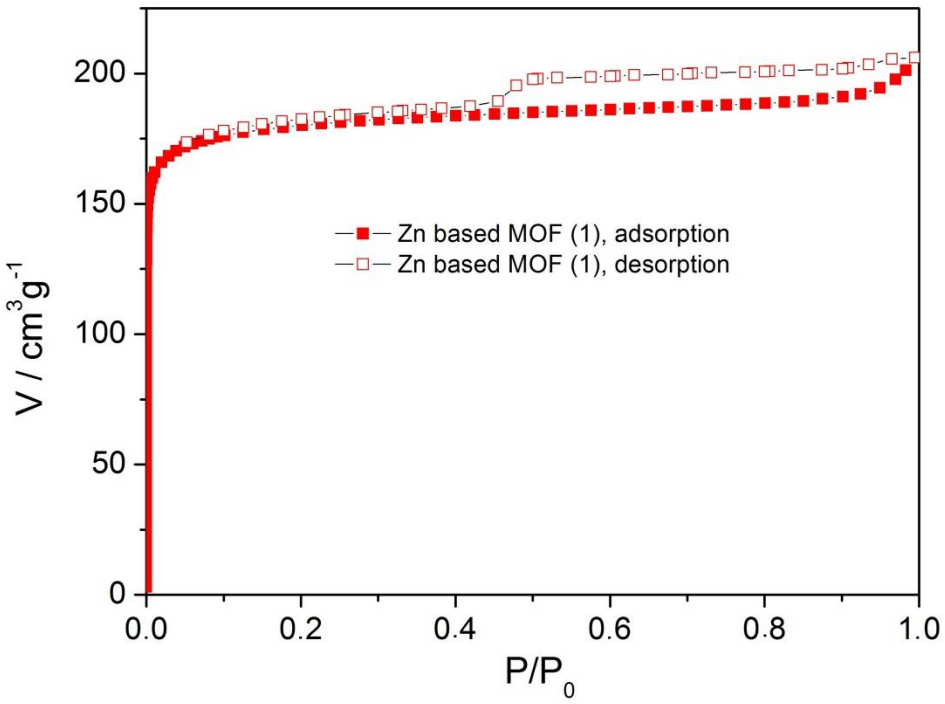

Figure 13. Nitrogen adsorption isotherms of **1** obtained from solvothermal synthesis (red) and at room temperature (black).

References

[1] (a) F. E. Arnold and J. P. Chen, *Rigid-rod benzobisazole polymer containing cyclic phosphate ester*, *US Patent*., US005200495A, Apr. 6, 1993; (b) D. Zhu, W. Bao, X. Wang, and X. Shen, *2,2´-Bisalkoxy-4,4´-biphenyl dicarboxylic acid and synthesis method thereof, China Patent*, CN101362688(A), Feb. 11, 2009; (c). H. Xu, W. Bao, Y. Xu, X. Liu, X. Shen, D. Zhu, *CrystEngComm*., 2012, **14**, 5720.

[2] S. Wöckel, *Diplomarbeit*, University of Leipzig, Germany, 2007.

[3] P. De Witte and J. Lemli, *J. Labelled Comp. Radiopharm*, 1987, **25**(1), 23.

[4] L. F. Tietze and Th. Eicher; Reaktionen and Synthesen, 1991, 2. Auflage, Georg Thieme Verlag, Stuttgart-New York, 156.

[5] H. Beckert, R. Beckert, G. Domschke and E. Fanghänel, *Organikum-Organisch-Chemisches Grundpraktikum*, 2001, 21.Auflage, Wiley-VCH, Weinheim, 238.

[6] T. Nagano and T. Hayashi, *Org.Lett*., 2005, **7**, 491.

[7] H. Becker, R. Beckert, G. Domschke and E. Fanghänel, *Organikum - Organisch-Chemisches Grundpraktikum*, 2001, 21. Auflage, Wiley-VCH, Weinheim, 562.

[8] P. Holý, P. Sehnal and M. Tichý, *Tetrahedron: Asymmetry*, 2003, **14**, 245.

[9] D. Dickie, G. Schatte, M. Jennings, S. Khoo and J. Clyburne, *Inorg. Chem.*, 2006, **45**, 1646.

[10] (a) Y. Zhao and D. Truhlar, *Theor. Chem. Acc.*, 2008, **120**, 215; (b) Y. Zhao and D. G. Truhlar, *Acc. Chem. Res.*, 2008, **41**, 157.

[11] M. J. Frisch, G. W. Trucks, H. B. Schlegel, G. E. Scuseria, M. A. Robb, J. R. Cheeseman, G. Scalmani, V. Barone, B. Mennucci, G. A. Petersson, H. Nakatsuji, M. Caricato, X. Li, H. P. Hratchian, A. F. Izmaylov, J. Bloino, G. Zheng, J. L. Sonnenberg, M. Hada, M. Ehara, K. Toyota, R. Fukuda, J. Hasegawa, M. Ishida, T. Nakajima, Y. Honda, O. Kitao, H. Nakai, T. Vreven, J. A. Montgomery Jr., J. E. Peralta, F. Ogliaro, M. Bearpark, J. J. Heyd, E. Brothers, K. N. Kudin, V. N. Staroverov, R. Kobayashi, J. Normand, K. Raghavachari, A. Rendell, J. C. Burant, S. S. Iyengar, J. Tomasi, M. Cossi, N. Rega, J. M. Millam, M. Klene, J. E. Knox, J. B. Cross, V. Bakken, C. Adamo, J. Jaramillo, R. Gomperts, R. E. Stratmann, O. Yazyev, A. J. Austin, R. Cammi, C. Pomelli, J. W. Ochterski, R. L. Martin, K. Morokuma, V. G. Zakrzewski, G. A. Voth, P. Salvador, J. J. Dannenberg, S. Dapprich, A. D. Daniels, O. Farkas, J. B. Foresman, J. V. Ortiz, J. Cioslowski, D. J. Fox, Gaussian 09, Revision A.02, Gaussian, Inc., Wallingford CT, 2009.

[12] (a) C. Peng and H. B. Schlegel, *Israel J. Chem.*, 1993, **33**, 449. (b) C. Peng, P. Y. Ayala, H. B. Schlegel and M. J. Frisch, *J. Comp. Chem.*, 1996, **17**, 49.

[13] H. McMurdie, M. Morris, E. Evans, B. Paretzkin, W. Wong-Ng, L. Ettlinger and C. Hubbard, *Powder Diffraction*, 1986, **1**, 76.